sciendo

DOI: 10.2478/auoc-2020-0021

Ovidius University Annals of Chemistry Volume 31, Number 2, pp. 122 - 131, 2020

Synthesis and characterization of magnetic oxide nanoparticles and corresponding thin films for wastewaters treatment

Lenuța CRINTEA (CĂPĂȚÂNĂ),[1] Viorica MUȘAT[*],[1] Silviu POLOSAN,[2] Alina CANTARAGIU,[3] Vasile BAȘLIU,[3] Andreea DEDIU (BOTEZATU), [4] and Rodica DINICĂ[4]

[1]*Laboratory of Chemical Nanotechnologies-LNC-CNMF, Dunărea de Jos" University of Galati, 47 Domnească Street, RO-800008, Galati, Romania*

[2]*Multifunctional Materials and Structures Laboratory, National Institute of Materials Physics, Atomistilor 405 A, 077125, Magurele, Romania*

[3]*Cross-border Faculty, Cahul, "Dunărea de Jos" University of Galati, 47 Domnească Street, RO-800008, Galati, Romania*

[4]*Department of Physical-Chemistry and Environment, "Dunărea de Jos" University of Galati, 47 Domnească Street, RO-800008, Galati, Romania*

Abstract. Industrial wastewater can be properly treated using nanotechnologies and nanomaterials. This paper presents the synthesis and characterization of three series of magnetic nanoparticles (MNPs) and corresponding thin films, used for the degradation of organic compounds and removal of heavy metals from industrial wastewater. The samples were obtained by co-precipitation from a ferric (Fe^{3+}) and ferrous (Fe^{2+}) ions solution in a molar ratio of 2:1, at temperatures between 80-95 °C. The characterization of the samples was performed by scanning electron microscopy (SEM), and X-ray diffraction (XRD) methods. The magnetic nanoparticles were deposited on glass substrates by the centrifugal coating technique and the optical and magneto-optical activity was investigated by UV-Vis spectroscopy and magnetic circular dichroism technique (MCD). The effect of the investigated samples on the decomposition under UV irradiation of organic dyes was monitored by UV-Vis spectroscopy. Our preliminary results have shown that the magnetite and maghemite MNPs can be effective in UV degradation of methylene blue (MB) dye.

Keywords: co-precipitation; magnetic nanoparticles; magnetic thin films; organic contaminants; wastewater.

1. Introduction

Current wastewater treatment technologies are efficient but costly and time consuming. Nanotechnology methods (chemical co-precipitation, ion exchange, reverse osmosis, electrochemical treatment and adsorption) [1] have the advantage of eliminating and recycling contaminants, reducing working time and expense [2]. Nanomaterials as metal oxides nanosorbents [3, 4], nano-photocatalysts, bioactive nanoparticles, nanostructured catalytic membranes [4], biomimetic membranes, molecular imprints polymers-MIP [5] and nanotechnologies represent a complex and comprehensive approach for removal of heavy metal ions, degradation of dissolved organic compounds and the fine suspensions.

Adsorption is the most recommended, efficient, economical, simple and used method [2] for removing organic and inorganic contaminants from wastewater [6]. Useful characteristics in adsorption, which recommend nanomaterials are: specific surface properties and high reactivity, high surface to volume ratio [6], adjustable pore size, hydrophilicity or hydrophobicity [7], high sorption capacity, superparamagnetism [6], high saturation field [8], very accessible adsorption sites, plasmonic resonance, quantum confinement effect [6].

Metal oxide MNPs are stable [9], can be easily functionalized with chemical compounds that increase their affinity for targeted contaminants [6], are highly selective for low concentration of pollutants and nontoxic [10]. Other advantages are low production cost and easy separation from pollutants [6]. Factors influencing the adsorption activity of metal oxide MNPs include pH [11, 12] (determines the ionization degree of the adsorbent molecule and the properties of the adsorbent surface [11]), the amount of adsorbent, the contact time [13], the selectivity and the binding rate for the contaminant [12, 14], the concentration of contaminants [11] and the temperature (the adsorption capacity decreases as temperature increases [11, 15, 16]).

Titanium dioxide [17, 18], zinc oxide, tungsten oxide [18] and alumina [17, 18]) have been proven efficient and economically advantageous [6] for the removal of heavy metals [17, 18] and radionuclides [17] by dissolving oxygen in contaminated water from complex metal oxides together with heavy metals [18]. Ferrous nano-oxides, are shown to be very efficient adsorbents for heavy metals, are inexpensive (widespread resources and simple synthesis),

[*]Corresponding author. *E-mail address*: Viorica.Musat@ugal.ro (Viorica Musat)

environmentally friendly and can be administered directly to contaminated sites, with negligible secondary contamination risks [19, 20].

Magnetic nanoparticles (NMP), such as maghemite (γ-Fe_2O_3), hematite (α-Fe_2O_3) and spinel ferrite ($M^{2+}Fe_2O_4$, where M^{2+} is Fe^{2+}, Cd^{2+}, Cu^{2+}, Ni^{2+}, Zn^{2+} or Mn^{2+}) are very good adsorption materials for collecting and removing arsenic, chromium, cobalt, copper, lead and nickel ions and can be easily separated by applying an external magnetic field [21-23].

The above-mentioned iron oxides-based MNPs can be obtained either by direct synthesis or by controlled oxidation/reduction methods [24]:

Magnetite (Fe_3O_4), also called *iron ferrite*, has a black or dark-gray color [25], contains both ferro (reduced) and ferric (oxidized) ion species known as iron oxide II and III, respectively [24], according to the reaction:

$$\underset{\text{(Ferrous Oxide)}}{FeO} + \underset{\text{(Ferric Oxide)}}{Fe_2O_3} \longrightarrow \underset{\text{(Magnetite)}}{Fe(II)O{\cdot}Fe_2(III)O_3}$$

Magnetite, sensitive to oxidation (transforming into maghemite by oxidation of Fe^{2+} ions), has a spinel cubic structure with a space of group Fd3m [25] and, due to the presence in the crystalline structure of the cations in two valence states (Fe^{2+} and Fe^{3+}), exhibits unique magnetic properties (superparamagnetism) [26].

The ferrite nanoparticles ($M^{2+}Fe_2O_4$) can be obtained by solution-based methods (co-precipitation, sol-gel, hydrothermal, sonochemical reactions) or by solid-state reaction (ball milling) followed by post-synthesis treatment, which also significantly influence their properties. The most widely used and simplest method for the synthesis of magnetic nanoparticles is the co-precipitation (first used by Massart) [27], at room or higher temperature, according to the following simplified reaction mechanism:

$$Fe^{2+} + 2Fe^{3+} + 8OH^- \leftrightarrows Fe(OH)_2 + 2Fe(OH)_3 \rightarrow Fe_3O_4\downarrow + 4H_2O$$

Maghemite (γ-Fe_2O_3) MNPs, with brown color, which can form by oxidation of magnetite, have a similar structure [25]. The γ-Fe_2O_3 nanoparticles coated with δ-FeOOH can remove chromium more effectively than uncoated ones [26]. Nano-goethite (α-FeOOH) and nano-hematite (α-Fe_2O_3) are efficient in adsorption of heavy metals [22] with a high adsorption capacity for Cu^{2+} ions (149.25 and 84.46 mg/g, respectively) and has a high photocatalytic activity [27].

Due to their biocompatibility and low toxicity, magnetite nanoparticles (Fe_3O_4) are also of particular interest due to their applications in biomedicine [28, 29], medical diagnosis [30], magnetic resonance imaging (MRI) [31], engineering tissue (Mag-TE) [32], magnetic hyperthermia [33, 34], bioseparation, immunological tests, biosensors [35], target drug-delivery [36, 37] and information storage [38]. The catalytic activity of MNPs has important applications in NH_3 reactions, alcohol oxidation, Fisher-Tropsch synthesis of hydrocarbons and in oxido-reduction reactions [39], car catalysts containing Pb^{2+} from the emitted gases [40]. Also, MNPs are used in analytical chemistry for isolation and enrichment of analytes in samples with a complex matrix (biological, food samples) [41], pigment industry [42] and for the absorption of heavy metals from water [43-47].

Photocatalysis is one of the most important properties of MNPs, used in the degradation of organic pollutants from waste, industrial or contaminated waters. The photocatalytic reaction is generally manifested in the presence of ultraviolet (UV) or infrared (IR) radiation [48], and represents a very promising method for degradation of a large number of organic (organic materials, organic acids, pesticides, dyes, crude oil), inorganic and biological (microbes, viruses, chlorine-resistant organisms) pollutants [49] from wastewater [50]. In this technique, the photocatalyst is the one that absorbs light and is involved in chemical reaction transformations [51]. For example, the photocatalyst nanocomposite containing maghemite (γ–Fe_2O_3) which can reduce chromium (VI) to chromium (III) from polluted waters, an inert and less toxic element and the photocatalyst nanocomposite with aluminum-silicate metal oxide can remove the ions. metals and organic contaminants [52].

In this paper, we present the synthesis and characterization of three series of magnetic nanoparticles (MNPs) and corresponding thin films by co-precipitation from a ferric (Fe^{3+}) and ferrous (Fe^{2+}) ions solution in a molar ratio of 2:1, at temperatures between 80-95 °C. Scanning electron microscopy (SEM), X-ray diffraction (XRD), optical spectroscopy and magneto-optical technique were used to characterize the morphology, particle size, crystalline phases, chemical structure and UV-VIS absorption of the investigated samples. The magneto-optical activity of the thin films was investigated by UV-Vis spectroscopy and magnetic circular dichroism technique (MCD). The use of these nanoparticles in water purification of organic and inorganic contaminants will be reported later in more detail.

2. Experimental

2.1. Synthesis of magnetic nanoparticles and thin films deposition

Three series (S1-S3) of MNPs were synthesized in the air by the co-precipitation from water solution, according to Jing - Fu Liu's method [53], at 80, 90 and 95 °C, respectively (Fig. 1). The reagents used in the synthesis of nanoparticles were ferric chloride hexahydrate ($FeCl_3{\cdot}6H_2O$), ferrous sulfate heptahydrate ($FeSO_4{\cdot}7H_2O$) and potassium hydroxide (KOH) with analytical quality, without further purification. The chemicals were purchased from Merck and Sigma-Aldrich.

The precipitation was performed at a pH of 12-12.5 under continuous stirring, resulting in a black, dark brown and brown suspension, depending on the working temperature (Fig. 1). After aging (60 min), the precipitates were separated from the mother solution, washed and dried 60 °C for 24 hours (Fig. 1).

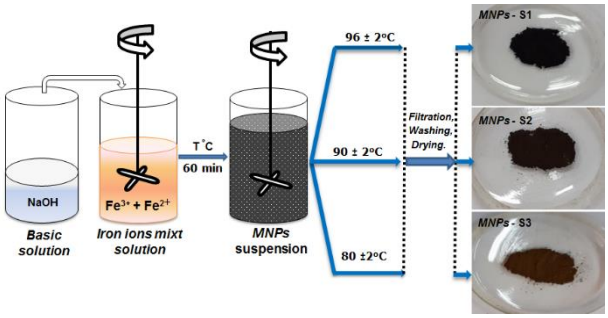

Figure 1. Steps of MNP synthesis

The thin film samples (noted F1-F3) were deposed on glass substrates by spin-coating, using an alcoholic dispersion (under US) of corresponding S1-S3 MNPs, at 500 rpm with three layers and dried at 90 °C for 10 min (see insets in Fig. 5).

2.2. Characterization of MNPs and thin films

The morphology of the investigated samples was highlighted by scanning electron microscopy (SEM) using a Quanta 200 (FEI) system. The preparation of MNPs samples for SEM examination consisted of air drying a drop of alcoholic dispersion of the nanoparticles (into an ultrasonic bath) onto a glass substrate and coated with a 5 nm thick Au layer by sputtering.

To investigate the crystalline structure and phase composition of the obtained MNPs, the X-ray diffraction (XRD) patterns of samples were recorded using a 3M DRON diffractometer (Russia) with CoK_α radiation, within the 2θ range between 15 and 90 degrees. The crystallite average sizes were calculated using the Debye-Scherrer formula:

$$d = \frac{k \cdot \lambda}{\beta \cdot \cos\theta},$$

where d is the average size of the crystallites (Å), λ - the wavelength of incident X-radiation (CoK_α) equal to 1.903 Å, k - constant with the value of 0.89, β- the full width of the peak at half its maximum intensity (FWHM)/measured in radians, θ - the diffraction angle for that intensity (the Bragg angle).

The preliminary magnetic behavior of the obtained nanoparticles was evidenced by the application of a magnetic field using "permanent" magnetic materials (Fig. 5).

The deposited thin films were characterized by determining the optical properties using UV-Vis spectroscopy for the identification of chemical species and the measurement of optical absorbance. Magneto-optical measurements evidence the main *d-d* transitions of iron ions for very weak or overlapping bands (Fig. 5), very helpful for the identification of the nanoparticle nature and crystalline structure [54]. In spite, the magnetic circular dichroism (MCD) underlines the transitions between ground and excited states of an ion in the crystal field (CF), highly sensitive to the magnetic ion site symmetry. These measurements were done with a JASCO 815 spectrometer equipped with a static magnet of 1.5 T and circularly polarized light from a 150W lamp. Light propagation was set parallel to the static magnetic field, and circular polarization was obtained using a photoelastic modulator capable of switching light polarization between right- and left-circular at a rate of 50 kHz. The MCD value was measured as the difference between the optical density of samples for the right and left polarized light relative to the magnetic field direction ($\Delta D = D+ - D-$) in the spectral range 700-300 nm at the temperature 300 K [55]. The samples were deposited on the glass substrates which have the bandgap at 300 nm.

The spectral dependencies of the circular magnetic dichroism in the visible range, for samples F1-F3, were measured at room temperature in the spectral range 300 - 700 nm.

The photocatalytic properties of the synthesized samples were investigated by UV-Vis spectroscopic monitoring of the degradation of methylene blue (MB) dye under UV irradiation using a UV lamp at KW 254 nm and LW 365 nm

3. Results and discussion

SEM images highlight the nanometric dimensions and morphology of the obtained nanoparticles. From Fig 2, one can notice a significant difference in the MNPs morphology. The S1 sample prepared at 95-97 °C (Fig. 2.a-c) shows both individual nanoparticles with dimensions between 30-90 nm, as well as aggregates up to 700-800 nm. The morphology of the S2 (90 °C) sample presents a homogeneous and compact self-assembling of individual spherical nanoparticles (Fig. 2.d-f) with an average diameter of 25 nm (~20-30 nm), while the S3 sample (80 °C) shows a totally different morphology. In the last case, overlapping platelets (2D nanostructure) with a diameter between about 20-70 nm, consisting of self-assemblings with floral and porous appearance were observed (Fig. 2.g-i). The 2D nanomorphology with increased surface area allows increased adsorption and functionalization of the MNPs.

Fig. 3 shows the X-ray diffraction patterns of the synthesized MNPs. According to these results, two main crystalline phases, in different proportions for each sample series, were identified: magnetite (Fe_3O_4) – space group P4332 and maghemite (γ-Fe_2O_3) - space group P 41212, with spinel cubic and tetragonal crystallization systems, respectively. The cubic goethite (FeO-OH) and rhombohedral wüstite (FeO) minority phases were also identified (Fig. 3 and Table 1).

The X-ray pattern of sample S1 shows intense peaks for five of the most important diffraction planes, (311), (400), (422), (440) and (515) of spinel cubic Fe_3O_4 structure, but also the planes (400) and (515) of γ-Fe_2O_3 spinel (Fig. 3.a), consistent with the results reported by Fangyuan Zhao *et al.* [56], Saumya Nigam *et al.* [57] and Anirban Roychowdhury *et al.* [58]. Figure 3.b shows for the sample S2 the diffraction planes (311) and (600) of the magnetite and (311), (400), (440) and (101) of the maghemite, according to Maryam *et al.* [59] and Y.H. Chen [60], while in the pattern of the sample S3 all diffraction peaks of the maghemite are clearly highlighted (Fig. 3.c), similar to other reported results [60, 61].

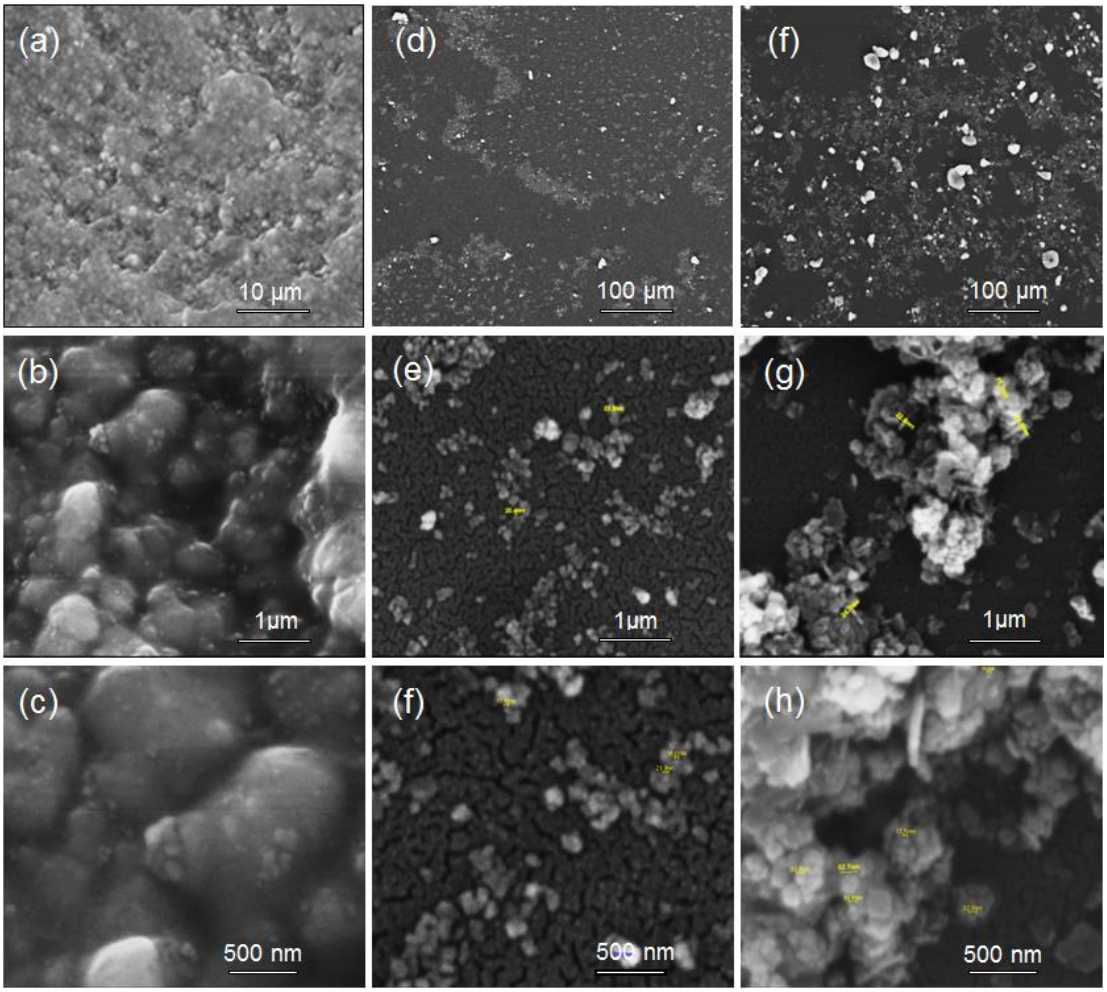

Figure 2. SEM images of MNPs S1 (a - c), S2 (d - f) and S3 (g - i)

From the quantitative analysis of the XRD data resulted that nanoparticles synthesized at 80 °C contain 85% maghemite and only 12% magnetite, those obtained at 90 °C contain the two magnetic phases in closed proportions (52 and 45%, respectively), while MNPs obtained at 95 °C consist of only 22% maghemite and ~73% magnetite. So, when the temperature of synthesis and aging increases, the amount of magnetite phase increases, by 33% when the temperature increase is from 80 to 90 °C and by another 28% when it reaches 95-97 °C (Table 1).

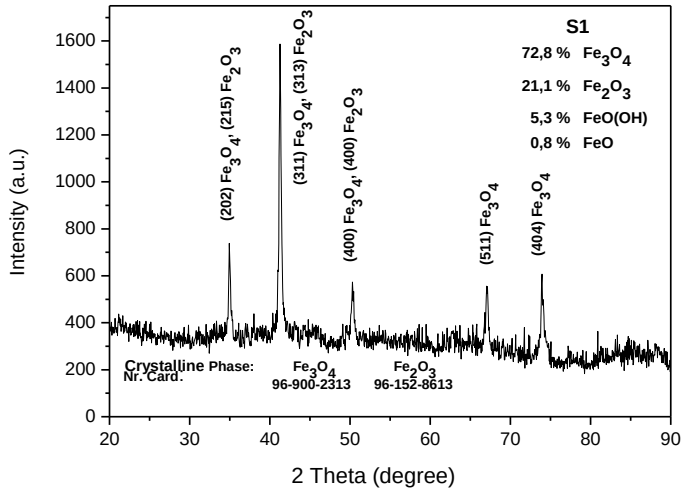

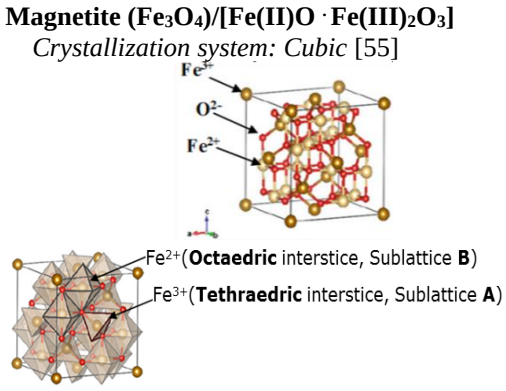

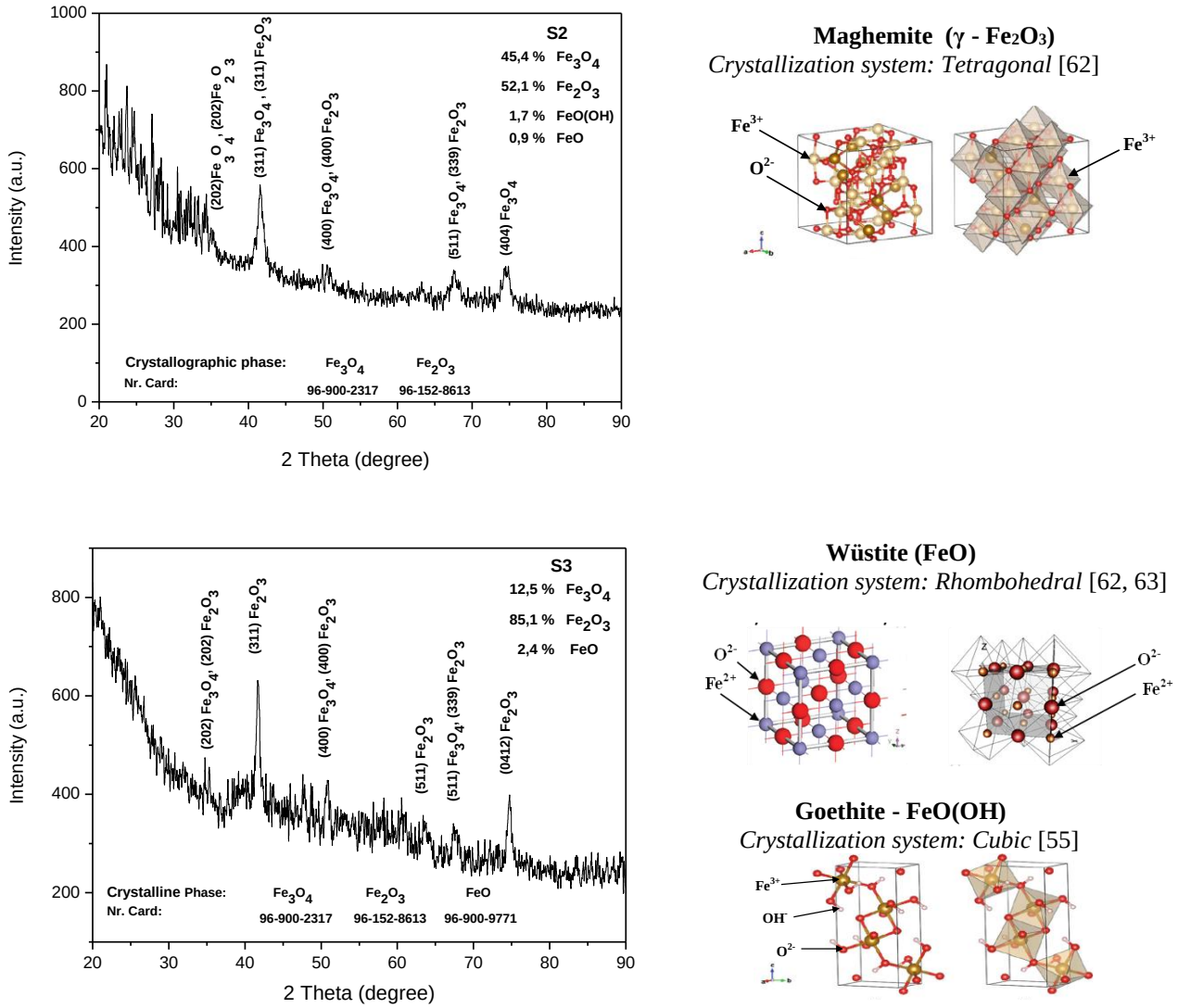

Figure 3. XRD patterns of the obtained MNS's samples (S1-S3), together with the representation of the crystalline structure of the identified magnetic components [55, 62, 63]

Table 1. Structural information for S1-S3 series (from XRD data)

No.	Crystalline phase	Structural parameters	S1	S2	S3
1.	**Fe_3O_4**	Phase composition (%) (Card number)	**72.8** (96-900-2313)	**45.4** (96-900-2317)	**12.5** (96-900-2317)
		Crystallites average size (nm)	30.7	24.1	23.0
2.	**Fe_2O_3**	Phase composition (%) (Card number)	**21.1** (96-152-8613)	**52.1** (96-152-8613)	**85.1** (96-152-8613)
		Crystallites average size (nm)	36.6	27.9	35.6
3.	**FeO**	Phase composition (%) (Card number)	**0.8** (96-900-9771)	**0.9** (96-900-9771)	**2.4** (96-900-9771)
		Crystallites average size (nm)	40.8	-	-
4.	**FeO(OH)**	Phase composition (%) (Card number)	**5.3** (96-434-4129)	**1.7** (96-434-4129)	-
		Crystallites average size (nm)	42.8	-	-

The photocatalytic effect of the synthesized samples, investigated by UV-Vis spectroscopic monitoring of the degradation of methylene blue (MB) dye in–aqueous solution under UV irradiation at LW 365 nm, are presented in Fig. 4.

The digital photographic images of the magnetic thin films, deposed from the alcoholic solutions of the S1-S3 MNPs series as shown in Fig. 5, together with the optical density in the UV-Vis range and magneto-optical properties using magnetic circular dichroism (MCD) technique.

The spectral dependencies of the magnetic circular dichroism in the visible range for samples F1-F3 were measured at room temperature in the spectral range 300 nm and 700 nm.

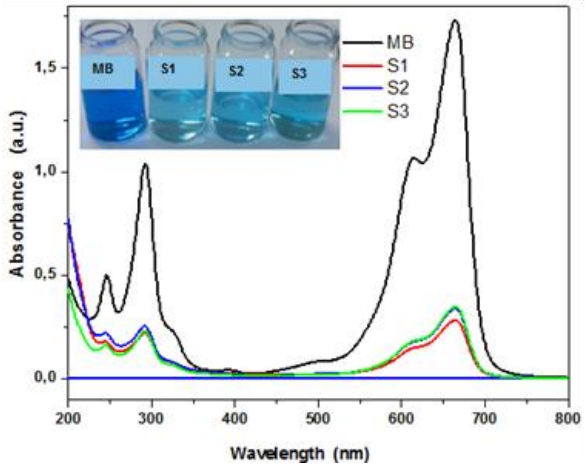

Figure 4. The degradation profile of MB in aqueous solution in the presence of the sample S1-S3

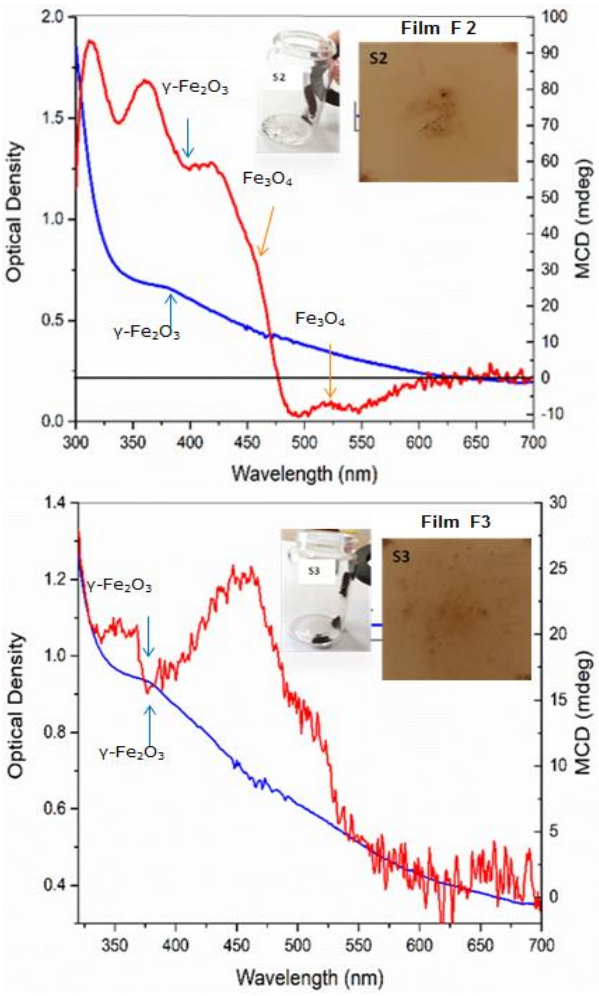

Figure 5. Magneto-optical properties of the magnetic thin films

The measured magneto-optical properties (Fig. 5) of the samples showed positive optical absorption spectra with a sharp onset of the band edges at 380 nm. In the F2 film sample, the spectrometer recorded positive optical absorption spectra of the band edge starting at a peak at 330 nm, having a high absorption at 370 nm for Fe_3O_4. The positive term of the MCD effect band was at 460 nm and the negative term of the MCD effect was observed at 530 nm indicating the presence of Fe_3O_4 crystals. At a wavelength of 385 nm, the optical absorption band is assigned to ɣ-Fe_2O_3 maghemite and the MCD effect band has a negative term. For the F3 film sample, the curve recorded a positive OD band and for the MCD effect band a negative peak at 385 nm, characteristic of ɣ-Fe_2O_3 crystals.

Magnetite (Fe_3O_4) crystallizes in the inverse spinel structure in which one-third of the Fe ions are surrounded by the four oxygen ions in the tetrahedral symmetry (A-site) while the other two-thirds of the Fe ions are surrounded by six oxygen atoms in the octahedral symmetry (B-site) (Fig. 6).

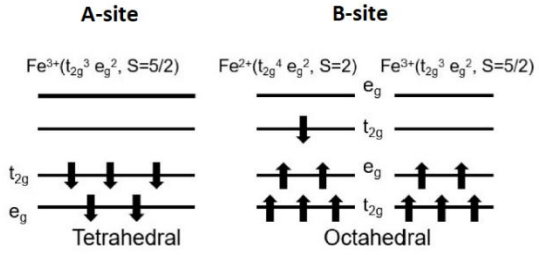

Figure 6. Electronic configurations of Fe^{2+} and Fe^{3+} in Fe_3O_4, in the two symmetries

While Fe^{2+} with electronic configuration $t_{2g}^4e_g^2$ (S=2) can be found only in the octahedral symmetry (B-site), the Fe^{3+} ions with electronic configurations $t_{2g}^3e_g^2$ (S=5/2) can be found in both symmetries, tetrahedral (spin-down) and octahedral (spin-up). Fe^{3+} is always paramagnetic due to the unpaired electrons in their orbitals, while Fe^{2+} bounded with oxygen atoms are strong-field ligands in an octahedral configuration with a low-spin density is created in the *d* orbitals. Apart from the direct $d-d$ charge transfer released from lattice distortion, oxygen atoms intermediated the intersite as well as the intrasite charge transfer through the overlapping $p-d$ orbital states [64]. In this context, the MCD peaks allow the identification between intersite transitions mediated by oxygen atoms and intrasite charge transfer transitions. The 530 nm (2.34 eV) is assigned to optical transition across the valence gap of the spin-majority (Fe^{3+}) between the B-site (e_g)↑ and A-site (e_g, t_{2g})↑. The second band from 460 nm (2.69 eV) may arise as an overlap between two transitions due to the intersystem charge transfer as a mixture of two transitions $[Fe^{2+}]e_g- \rightarrow [Fe^{3+}]e$; $[Fe^{3+}]t_2- \rightarrow [Fe^{2+}]t_{2g}$ [65]. The third transition at around 385 nm (3.22 eV) arises from the Fe^{2+} in the B-site as $[Fe^{2+}]t_{2g} \rightarrow [Fe^{2+}]e_g$ [66]. The one at 370 nm (3.35 eV) arises as an overlap between Fe_3O_4 given by $[Fe^{2+}]t_{2g} \longrightarrow [Fe^{3+}]e$ as intervalence charge transfer (weak band) with the stronger band of the diamagnetic term of ɣ-Fe_2O_3 having a negative sign in MCD.

4. Conclusions

Three series of magnetic oxide nanoparticles (MNPs), were obtained by co-precipitation from a mixed ferrous-ferric ions solution at temperatures between 80-97 °C. Thin films were deposited on glass substrates by the centrifugal coating technique using the corresponding alcoholic dispersions of the three series of oxide MNPs.

SEM images highlighted significant differences in the MNPs morphology. The three series prepared at 95-97 °C, 90 °C and 80 °C show individual nanoparticles (30-90 nm) together with aggregates up to 700-800 nm, homogeneous and compact self-assembling of individual spherical nanoparticles (~20-30 nm) and overlapping platelets (2D nanostructure) with diameter between ~20-70 nm, respectively

The XRD data showed that the samples obtained at the highest (~97 °C) and lowest temperature (~ 80 °C) mostly consists of cubic magnetite (Fe_3O_4, 73%) and tetragonal maghemite (γ-Fe_2O_3, 85%) phases, respectively. At ~90 °C, the MNPs consist of a mixture of these two phases in closed proportions.

The MCD spectra confirmed the presence of ferromagnetic magnetite phases highlighted by XRD data, together with the maghemite phase, which magnetic properties, depending on the particle size, are paramagnetic or superparamagnetic when larger or smaller than 10 nm, respectively.

The spin-majority configuration (Fe^{3+}) is given by the paramagnetic transition from 530 nm (2.34 eV) seconded by the intersystem charge transfer between Fe^{3+} and Fe^{2+} in the A and B sites, centered at 460 nm. The third intersystem charge transfer appears at 370 nm (3.35 eV) identify a Fe^{2+}- Fe^{3+} optical absorption which is overlapped to the diamagnetic transition of Fe^{2+} in ɣ-Fe_2O_3. The fourth transition at around 385 nm (3.22 eV) arises from the Fe^{2+} in the B-site as $[Fe^{2+}]t_{2g} \rightarrow [Fe^{2+}]e_g$.

Our preliminary study has shown that magnetic nanoparticles of magnetite and maghemite can be effective in UV and VIS degradation of MB dye.

Conflict of interest

The authors declare that there is no conflict of interest regarding the publication of this article.

References

[1]. Z. Elouear, J. Bouzid, N. Boujelben, M. Feki, F. Jamoussi, A. Montiel, Heavy metal ions removal from aqueous solutions by activated phosphate rock, Journal of Hazardous Materials 156 (2008) 412-420. DOI: 10.1016/j.jhazmat.2007.12.036

[2]. S. Kanchi, Nanotechnology for water treatment, Journal Environmental Analytical Chemistry 1 (2014) 1-3. DOI: 10.4172/2380-2391.1000e102

[3]. I. Ali, New generation adsorbents for water treatment, Chemical Reviews 112 (2012) 5073-5091. DOI: 10.1021/cr300133d

[4]. I. Gehrke, A. Geiser, A. Somborn-Schulz, Innovations in nanotechnology for water treatment, Nanotechnology, Science and Applications 8 (2015) 1-17. DOI: 10.2147/NSA.S43773

[5]. G. Xu, L. Yang, M. Zhong, C. Li, X. Lu, X. Kan, Selective recognition and electrochemical detection of p-nitrophenol based on a macroporous imprinted polymer containing gold nanoparticles, Microchim Acta 180 (2013) 1461-1469. DOI: 10.1007/s00604-013-1090-8

[6]. X. Qu, P. J. J. Alvarez, Q. Li, Applications of nanotechnology in water and wastewater treatment, Water Research 47 (2013) 3931-3946. DOI: 10.1016/j.watres.2012.09.058

[7]. R. Das, A.M.E. Hamid, S.B.A. Ramakrishna, S. Chowdhury, Z. Zaman, Carbon nanotube membranes for water purification: a bright future in water desalination, Desalination 336 (2014) 97-109. DOI: 10.1016/j.desal.2013.12.026

[8]. X. Batlle, A. Labarta, Finite-size effects in fine particles: magnetic and transport properties, Journal of Physics D: Applied Physics 35 (2002) R15. DOI: 10.1088/0022-3727/35/6/201

[9]. X. Qu, J. Brame, Q. Li, P.J.J. Alvarez, Nanotechnology for a safe and sustainable water supply: enabling integrated water treatment and reuse, Accounts of Chemical Research 46 (2013) 834-843. DOI: 10.1021/ar300029v

[10]. T.E. Cloete, M. de Kwaadsteniet, M. Botes, J.M. López-Romero, Nanotechnology in Water Treatment Applications, Caister Academic Press, Norfolk, UK (2010).

[11]. M.T. Yagub, T.K. Sen, S. Afroze, H.M. Ang, Dye and its removal from aqueous solution by adsorption: a review, Advances in Colloid and Interface Science 209 (2014) 172-184. DOI: 10.1016/j.cis.2014.04.002

[12]. E.N. Zare, M.M. Lakouraj, A. Ramezani, Efficient sorption of Pb (II) from an aqueous solution using a poly (aniline-co-3-aminobenzoic acid)-based magnetic core–shell nanocomposite, New Journal of Chemistry 40 (2016) 2521-2529. DOI: 10.1039/C5NJ02880A

[13]. Y. Bulut, H. Aydın, A kinetics and thermodynamics study of methylene blue adsorption on wheat shells, Desalination 194 (2006) 259-267. DOI:10.1016/j.desal.2005.10.032

[14]. A.G. Yavuz, E.D. Atalay, A. Uygun, F. Gode, E. Aslan, A comparison study of adsorption of Cr(VI) from aqueous solutions onto alkyl-substituted polyaniline/chitosan composites, Desalination 279 (2011) 325-331. DOI:10.1016/j.desal.2011.06.034

[15]. M.E. Argun, S. Dursun, M. Karatas, M. Gürü, Activation of pine cone using Fenton oxidation for Cd(II) and Pb(II) removal, Bioresource Technology 99 (2008) 8691–8698. DOI: 10.1016/j.biortech.2008.04.014

[16]. S. Netpradit, P. Thiravetyan, S. Towprayoon, Adsorption of three azo reactive dyes by metal hydroxide sludge: effect of temperature, pH, and electrolytes, Journal of Colloid and Interface Science 270 (2004) 255-261. DOI: 10.1016/j.jcis.2003.08.073

[17]. D. Koeppenkastrop, E.H. Decarlo, Uptake of rare-earth elements from solution by metal-oxides, Environmental Science and Technology 27 (1993) 1796-1802. DOI:10.1021/es00046a006

[18]. P. Trivedi, L. Axe, Modeling Cd and Zn sorption to hydrous metal oxides, Environmental Science and Technology 34 (2000) 2215-2223. DOI: 10.1021/es991110c

[19]. Y.H. Li, J. Ding, Z. Luan, Z. Di, Y. Zhu, C. Xu, D. Wu, B. Wei, Competitive adsorption of Pb^{2+}, Cu^{2+} and Cd^{2+} ions from aqueous solutions by multiwalled carbon nanotubes, Carbon 41 (2003) 2787-2792. DOI: 10.1016/S0008-6223(03)00392-0

[20]. Y.H. Li, S. Wang, Z. Luan, J. Ding, C. Xu, D. Wu, Adsorption of cadmium(II) from aqueous solution by surface oxidized carbon nanotubes, Carbon 41 (2003) 1057-1062. DOI: 10.1016/S0008-6223(02)00440-2

[21]. A.Z.M. Badruddoza, Z.B.Z. Shawon, M.T. Rahman, K.W. Hao, K. Hidajat, M.S. Uddin, Ionically modified magnetic nanomaterials for arsenic and chromium removal from water, Chemical Engineering Journal 225 (2013) 607-615. DOI: 10.1016/j.cej.2013.03.114

[22]. Y. Lei, F. Chen, Y. Luo, L. Zhang, Three-dimensional magnetic graphene oxide foam/Fe_3O_4 nanocomposite as an efficient absorbent for Cr(VI) removal, Journal of Materials Science 49 (2014) 4236–4245. DOI: 10.1007/s10853-014-8118-2

[23]. L. Tan, J. Xu, X. Xue, Z. Lou, J. Zhu, S.A. Baig, X. Xu, Multifunctional nanocomposite Fe_3O_4@SiO_2-mPD/SP for selective removal of Pb(II) and Cr(VI) from aqueous solutions, Royal Society of Chemistry Advances 4 (2014) 45920-45929. DOI: 10.1039/c4ra08040h

[24]. R.M. Fratila, S.G. Mitchell, P. del Pino, V. Grazu, J.M. de la Fuente, Strategies for the biofunctionalization of gold and iron oxide nanoparticles, Langmuir 30 (2014) 15057-15071. DOI: 10.1021/la5015658

[25]. R.R. Baker, J.G. Mather, J.H. Kennaugh, Magnetic bones in human sinuses, Nature 301 (1983) 79-80. DOI: 10.1038/301078a0

[26]. W. Wu, Z. Wu, T. Yu, C. Jiang, W.S. Kim, Recent progress on magnetic iron oxide nanoparticles: synthesis, surface functional strategies and biomedical applications, Science and Technology of Advanced Materials 16 (2015) e023501 (43pp). DOI: 10.1088/1468-6996/16/2/023501

[27]. Y.H. Chen, F.A. Li, Kinetic study on removal of copper(II) using goethite and hematite nano-photocatalysts, Journal of Colloid and Interface Science 347 (2010) 277-281. DOI: 10.1016/j.jcis.2010.03.050

[28]. P. Majewski, B. Thierry, Functionalized magnetite nanoparticles-synthesis, properties, and bio-applications, Critical Reviews in Solid State and Materials Sciences 32 (2007) 203-215. DOI: 10.1080/10408430701776680

[29]. P.J. Tarta, M.P. Morales, T.G. Xlez-Carreno, S. Veintemillas-Verdaguer, C.J. Serna, Advances in magnetic nanoparticles for biotechnology applications, Journal of Magnetism and Magnetic Materials 290-291 (2005) 28-34. DOI: 10.1016/j.jmmm.2004.11.155

[30]. D.C. Culita, G. Marinescu, L. Patron, O. Carp, C. B. Cizmas, L. Diamandescu, Superparamagnetic nanomagnetites modified with histidine and tyrosine, Materials Chemistry and Physics 111 (2008) 381–385. DOI: 10.1016/j.matchemphys.2008.04.033

[31]. D.E. Speliotis, Magnetic recording beyond the first 100 Years, Journal of Magnetism and Magnetic Materials 193 (1999) 29-35. DOI: 10.1016/S0304-8853(98)00399-0

[32]. A. Ito, M. Hayashida, H. Honda, K. Hata, H. Kagami, M. Ueda, T. Kobayashi, Construction and harvest of multilayered keratonocyte sheets using magnetite nanoparticles and magnetic force, Tissue Engineering 10 (2004) 873-880. DOI: 10.1089/1076327041348446

[33]. A. Jordan, P. Wust, H. Fahling, R. Scholz, Inductive heating of ferrimagnetic particles and magnetic fluids: Physical evaluation of their potential for hyperthermia, international journal of hyperthermia 9 (1993) 51-58. DOI: 10.3109/02656739309061478

[34]. U. Hafeli, W. Schutt, J. Teller, M. Zborowski, Scientific and Clinical Applications of Magnetic Carriers, Springer Science et Bussiness Media, Plenum Press: New York and London (1997) 527-534.

[35]. W. Wu, Z. Wu, T. Yu, C. Jiang, W.S. Kim, Recent progress on magnetic iron oxide nanoparticles: synthesis, surface functional strategies and biomedical applications, Science and Technology of Advanced Materials 16 (2015) 023501. DOI: 10.1088/1468-6996/16/2/023501

[36]. P.K. Gupta, C.T. Hung, F.C. Lam, D.G. Perrier, Albumin Microspheres. III. Synthesis and characterization of microspheres containing adriamycin and magnetite, International Journal of Pharmaceutics 43 (1988) 167-177. DOI: 10.1016/0378-5173(88)90072-5

[37]. T. Neuberger, B. Schopf, H. Hofmann, M. Hofmann, B. von Rechenberg, Superparamagnetic nanoparticles for biomedical applications: possibilities and limitations of a new drug delivery system, Journal of Magnetism and Magnetic Materials 293 (2005) 483-496. DOI: 10.1016/j.jmmm.2005.01.064

[38]. Z. Xu, Y. Hou, S. Sun, Magnetic core/shell Fe_3O_4/Au and Fe_3O_4/Au/Ag nanoparticles with tunable plasmonic properties, Journal of the American Chemical Society 129 (2007) 8698-8699. DOI: 10.1021/ja073057v

[39]. Q. Liu, Z.M. Cui, Z. Ma, S.W. Bian, W.G. Song, L.J. Wan, Morphology control of Fe_2O_3 nanocrystals and their application in catalysis, Nanotechnology 18 (2007) 385605. DOI: 10.1088/0957-4484/18/38/385605

[40]. A.M. Grumezescu, Water purification/ Nanotechnology in the Agri-Food Industry, Academic Press Volume 9/ 8 Chapter 1 (2017). ISBN: 978-0-12-804300-4

[41]. M. Wierucka, M. Biziuk, Application of magnetic nanoparticles for magnetic solid-phase extraction in preparing biological, environmental and food

samples, TrAC Trends in Analytical Chemistry 59 (2014) 50-58. DOI: 10.1016/j.trac.2014.04.007

[42]. J.H. Meg, G.Q. Yang, L.M. Yan, X.Y. Wang, Synthesis and characterization of magnetic nanometer pigment Fe_3O_4, Dyes and Pigments 66 (2005) 109-113. DOI: 10.1016/j.dyepig.2004.08.016

[43]. A.F.C. Campos, R. Aquino, T.A.P.G. Cotta, F.A. Tourinho, J. Depeyrot, Using speciation diagrams to improve synthesis of magnetic nanosorbents for environmental applications, Bulletin of Materials Science 34 (2011) 1357-1361. DOI: 10.1007/s12034-011-0328-5

[44]. P. Russo, D. Acierno, M. Palomba, G. Carotenuto, R. Rosa, A. Rizzuti, C. Leonelli, Ultrafine magnetite nanopowder: Synthesis, characterization, and preliminary use as filler of polymethylmethacrylate nanocomposites, Journal of Nanotechnology, 2012 (2012) e728326. DOI: 10.1155/2012/728326

[45]. H. Karami, Heavy metal removal from water by magnetite nanorods, Chemical Engineering Journal 219 (2013) 209-216. DOI: 10.1016/j.cej.2013.01.022

[46]. H. Karami, E. Chidar, Pulsed-electrochemical synthesis and characterizations of magnetite nanorods, International Journal of Electrochemical Science 7 (2012) 2077-2090. http://www.electrochemsci.org/papers/vol7/7032077.pdf

[47]. S. Malato, P.F. Ibanez, M.I. Maldonado, J. Blanco, W. Gernjak, Decontamination and disinfection of water by solar photocatalysis: Recent overview and trends, Catalysis Today 147 (2009) 1-59. DOI: 10.1016/j.cattod.2009.06.018

[48]. D. Rickerby, M. Morrison, Report from the workshop on nanotechnologies for environmental remediation, JRC Ispra 2007 (2011), from: http://www.nanowerk. com/nanotechnology/reports/reportpdf/report101.pdf

[49]. J. Bandara, U. Klehm, J. Kiwi, Raschig rings-Fe2O3 composite photocatalyst activate in the degradation of 4-chlorophenol and Orange II under daylight irradiation. Applied Catalysis B: Environmental 76 (2007) 73-81. DOI: 10.1016/j.apcatb.2007.05.007

[50]. A.D. McNaught, A. Wilkinson, IUPAC Gold Book, Blackwell Scientific Publications, Oxford (1997).

[51]. K. Jones, C. Boxall, R. McCabe, D. Shaw, M. Buck, Nanocomposites for water treatment, ECS Transactions 6 (2007) 17-27. DOI: 10.1149/1.2790398

[52]. J.F. Liu, Z.S. Zhao, G.B. Jiang, Coating Fe_3O_4 magnetic nanoparticles with humic acid for high efficient removal of heavy metals in water, Environmental Science & Technology 42 (2008) 6949-6954. DOI: 10.1021/es800924c

[53]. M. dos Santos Pires, L.C. Tavares Lacerda, S. Corrêa, T.C. Silva, A.A. de Castro, T.C. Ramalho, Iron Oxides Applied to Catalysis, Recent Advances in Complex Functional Materials Spinger, 2017, pp. 409-42. DOI: 10.1007/978-3-319-53898-3_16

[54]. I. Edelman, O. Ivanova, R. Ivantsov, D. Velikanov, V. Zabluda, Y. Zubavichus, A. Veligzhanin, V. Zaikovskiy, S. Stepanov, A. Artemenko, J. Curély, J. Kliava, Magnetic nanoparticles formed in glasses co-doped with iron and larger radius elements, Journal of Applied Physics, 112 (2012) e084331. DOI: 10.1063/1.4759244

[55]. D.A. Petrov, R.D. Ivantsov, S.M. Zharkov, D.A. Velikanov, M.S. Molokeeva, C.R. Lin, C.T. Tso, H.S. Hsu, Y.T. Tseng, E.S. Lin, I.S. Edelman, Magnetic and magneto-optical properties of Fe_3O_4 nanoparticles modified with Ag, Journal of Magnetism and Magnetic Materials 493 (2020) 165692. DOI: 10.1016/j.jmmm.2019.165692

[56]. F. Zhao, B. Zhang, L. Feng, Preparation and magnetic properties of magnetite nanoparticles, Materials Letters 68 (2012) 112–114. DOI: 10.1016/j.matlet.2011.09.116

[57]. S. Nigam, K. C. Barick, D. Bahadur, Development of citrate-stabilized Fe_3O_4 nanoparticles: Conjugation and release of doxorubic in for therapeutic applications, Journal of Magnetism and Magnetic Materials 323 (2011) 237–243. DOI: 10.1016/j.jmmm.2010.09.009

[58]. A. Roychowdhury, S. Prakash Pati, S. Kumar, D. Das, Effects of magnetite nanoparticles on optical properties of zinc sulfide in fluorescent-magnetic Fe_3O_4/ZnS nanocomposites, Powder Technology 254 (2014) 583–590. DOI: 10.1016/j.powtec.2014.01.076

[59]. M.F.K. Ariffin, A. Idris, N.H.A. Ngadiman, Optimization of lipase immobilization on maghemite and its physico-chemical properties, Brazilian Journal of Chemical Engineering 36 (2019) 171–179. DOI: 10.1590/0104-6632.20190361s20180168

[60]. Y.H. Chen, Thermal properties of nanocrystalline goethite, magnetite, and maghemite, Journal of Alloys and Compounds 553 (2013) 194–198. DOI: 10.1016/j.jallcom.2012.11.102

[61]. L. Li, L.J. Yuan, W. Hong, L. Fan, L.B. Mao, L. Liu, Hybrid Fe_3O_4/MOFs for the adsorption of methylene blue and methyl violet from aqueous solution, Desalination and Water Treatment 55 (2015) 1973–1980. DOI: 10.1080/19443994.2014.937751

[62]. N. Quijorna, M. de Pedro, M. Romero, A. Andrés, Characterisation of the sintering behaviour of Waelz slag from electric arc furnace (EAF) dust recycling for use in the clay ceramics industry, Journal of Environmental Management 132 (2014) 278-286. DOI: 10.1016/j.jenvman.2013.11.012

[63]. X. Yu, J. Zhou, Grain boundary in oxide scale during high-temperature metal processing, *in* Study of Grain Boundary Character, pp 59-77, IntechOpen (2017). DOI: 10.5772/66211

[64]. J. Chen, H.S. Hsu, Y.H. Huang, Spin-dependent optical charge transfer in magnetite from transmitting optical magnetic circular dichroism, Physical Review B 98 (2018) e085141. DOI: 10.1103/PhysRevB.98.085141

[65]. J. Chen, H.S. Hsu, Y.H. Huang, Spin-dependent optical charge transfer in magnetite from transmitting optical magnetic circular dichroism, Physical Review B 98 (2018) 085141. DOI: 10.1103/PhysRevB.98.085141
[66]. K.J. Kim, H.S. Lee, M.H. Lee, S.H. Lee, Comparative magneto-optical investigation of d–d charge–transfer transitions in Fe_3O_4, $CoFe_2O_4$, and $NiFe_2O_4$, Journal of Applied Physics 91 (2002) 9974. DOI: 10.1063/1.1480482

Received: 09.09.2020
Received in revised form: 10.10.2020
Accepted: 10.10.2020